Eur J Nucl Med Mol Imaging (2009) 36 (Suppl 1):S15–S29
DOI 10.1007/s00259-008-1016-6

Multimodality imaging: an update on PET/CT technology

Osama Mawlawi · David W. Townsend

Published online: 23 December 2008

Abstract
Introduction Since their introduction in 2001, PET/CT systems have gained wide acceptance primarily due to their inherent ability to combine functional and structural information about the underlying disease state of the patient in a single imaging session. Their significance has also been documented with regard to their short imaging times, which minimize patient anxiety and image blurring due to patient motion. In the past seven years, PET/CT systems have replaced dedicated PET systems as the imaging modality of choice for diagnostic evaluation of oncology patients.
Objectives The purpose of this article is to review the evolution of PET/CT systems and document their current status.
Discussion Recent improvements in instrumentation are highlighted together with some outstanding issues that arise for specific PET/CT applications. These are followed by a description of some of the more common clinical applications of PET/CT imaging such as staging malignant disease, treatment planning, and monitoring therapy response. Finally, the future developments of PET/CT systems with regard to sensitivity, resolution, and new radiopharmaceuticals are discussed. The article concludes by presenting some issues concerning the next stage in the future of PET imaging, namely PET/MRI.

O. Mawlawi (✉)
Department of Imaging Physics, MD Anderson Cancer Center,
Box 1352, Houston, TX 77030, USA
e-mail: omawlawi@mdanderson.org

D. W. Townsend
Medicine, University of Tennessee Graduate School of Medicine,
1924 Alcoa Highway,
Knoxville, TN 37920, USA
e-mail: dtownsend@mc.utmck.edu

Keywords PET/CT · Multimodality imaging · Time of flight · Motion correction · Lesion segmentation · Partial volume averaging · Therapy planning · PET/MRI

Introduction

The first commercial PET/CT system appeared in the clinic in 2001 following the introduction of a prototype design in 1998 [1]. The clinical evaluation of the prototype from 1998 to 2001 [2–4] at the University of Pittsburgh Medical Center unquestionably highlighted the advantages of multimodality imaging and especially the routine availability of coregistered anatomical and functional images when scanning oncology patients. The ability to accurately localize functional abnormalities and to assess the functionality of anatomical structures proved to be a significant advance for clinical imaging. Despite initial concerns relating to device cost and ownership, the approach was rapidly embraced by a medical profession increasingly receptive to the benefits of whole-body dual-modality imaging. By 2006, the major vendors no longer offered PET-only systems, and PET/CT became an established imaging technology. Advances in CT and PET instrumentation could be incorporated directly into PET/CT, thus, ensuring state-of-the-art functionality for both modalities in the combined device. Consequently, by mid-2008, over 3,000 combined PET/CT systems were in clinical operation worldwide. While most PET/CT applications are for staging malignant disease, and increasingly, for therapy planning and monitoring response, the incorporation of high-performance CT components suggests potential applications for cardiac PET/CT. With such high-performance CT and PET components, whole-body FDG-PET/CT examinations are now completed for staging purposes in 10 min, or less.

The purpose of this article is to briefly review the current status of CT and PET, and the integration into a combined PET/CT device. Recent improvements in instrumentation are described together with some outstanding issues that arise for specific PET/CT applications. Finally, some of the more common clinical applications for staging malignant disease, planning treatment and monitoring therapy response are discussed.

Design aspects of PET/CT

The development of the first PET/CT prototype device was initiated in 1992 with the objectives to integrate CT and PET within the same device and to use the CT images for attenuation and scatter correction of the PET emission data. The goal was to construct a device with both clinical CT and clinical PET capability so that a full anatomical and functional scan could be acquired in a single session, obviating the need for the patient to undergo an additional clinical CT scan. The original prototype [1] combined a single-slice spiral CT scanner (Somatom AR.SP; Siemens Medical Solutions, Germany) with a rotating ECAT ART PET system (CPS Innovations, Knoxville, TN).

Despite concerns over the likely cost and operational complexity of combined PET/CT technology, the major vendors of medical imaging equipment nevertheless recognized a market for PET/CT. The first commercial design (Discovery LS, GE Healthcare, Waukesha, WI) comprised a CT and a PET enclosed within a single gantry cover and operated from separate consoles. The design involved little integration at any level and was intended primarily to be the first commercial PET/CT system on the market, as indeed it was. The PET components included retractable septa and standard PET transmission sources were offered as an alternative to CT-based attenuation correction. Retractable septa allowed the device to acquire PET data in either 2-D or 3-D mode. Within a few months, another PET/CT system design (Fig. 1) was proposed by Siemens ICTI (Knoxville, Tenn) that had no septa and acquired data fully in 3-D [5]. Since no mechanical storage was required for retractable septa and standard PET transmission sources were not offered, the design was compact; the patient port was a full 70 cm diameter throughout and the overall tunnel length was only 110 cm. Integration of the control and display software allowed the PET/CT scanner to be operated from a single console.

The hardware integration of recent PET/CT system designs has, therefore, remained rather minimal. The advantage is that vendors can then benefit more easily from separate advances in both CT and PET instrumentation. In the past few years, spiral CT technology has progressed from single to dual-slice, to 4, 8, 16 and, most recently, 64 slices; in parallel, CT rotation times have deceased to less than 0.4 s resulting in very rapid scanning protocols. Advances in PET technology have been equally dramatic with the introduction of new faster scintillators such as gadolinium oxyorthosilicate (GSO) and lutetium oxyorthosilicate (LSO), faster acquisition electronics and higher resolution detectors (smaller pixels). Currently, a top-of-the-line PET/CT configuration might comprise a 64-slice CT scanner and an LSO-based PET with 4-mm detector elements. However, while the 64-slice CT configuration is targeted primarily for cardiac applications, the greatest impact of PET/CT to date has been in the oncology field.

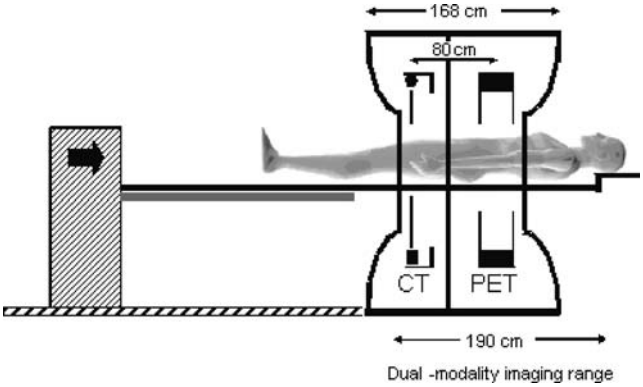

Fig. 1 Schematic of an early PET/CT system design. The CT scanner is positioned in front of the PET system and the centers of the imaging fields are separated by 80 cm field-of-view. To maximize the co-scan range (the range covered by both CT and PET), the movement of the bed must include the 80 cm FOV separation. A typical co-scan range is 160–190 cm. The patient port is 70 cm, thereby reducing the claustrophobic effect of the extended gantry dimensions

Current status of PET/CT systems

Currently five vendors offer PET/CT designs: GE Healthcare, Hitachi Medical, Philips Healthcare, Toshiba Medical Corporation and Siemens Medical Solutions. The exact specifications and performance of the CT and PET components are vendor-specific, as shown in Fig. 2.

The Gemini, SceptreP3, Aquiduo and Biograph designs acquire PET data in 3-D mode only, whereas the Discovery incorporates retractable septa and can acquire data in both 2-D and 3-D mode. While the debate continues as to whether 2-D or 3-D acquisition yields better image quality, particularly for large patients, significant improvement in 3-D image quality has undoubtedly been achieved through the use of faster scintillators and statistically-based reconstruction algorithms. The scintillators GSO (Gemini GXL), LSO (SceptreP3, Aquiduo and Biograph), and LYSO (Gemini TF and Discovery RX) result in lower rates of both scattered photons and random coincidences compared to BGO and offer superior performance for 3-D whole-body imaging.

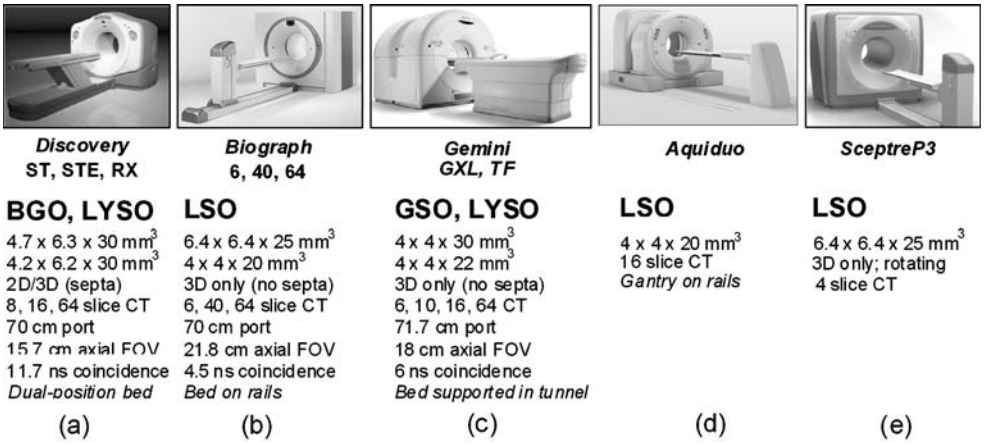

Fig. 2 Biograph range. Current PET/CT designs from the five major suppliers of medical imaging equipment: (**a**) the GE Healthcare Discovery range, (**b**) the Siemens Biograph True-Point, (**c**) the Philips Gemini series, and (**d**, **e**) two designs from Japanese vendors, the Toshiba Aquiduo and the Hitachi SceptreP3; both Japanese designs incorporate PET components developed by Siemens

While there has, to date, been little actual effort to increase the level of hardware integration, there has been significant effort to reduce the complexity and increase the reliability of system operation by adopting a more integrated software approach. In early designs, CT and PET data acquisition and image reconstruction were performed on separate systems accessing a common database. Increasingly, functionality has been combined so as to reduce cost and complexity and increase reliability. Similar considerations of cost and complexity for the hardware may lead, in the future, to greater levels of integration. The likelihood is that these designs will be application-specific, incorporating a 16-slice CT scanner for oncology and a 64-slice (or higher) CT scanner for cardiology. There will potentially be a demand for more cost-effective entry-level PET/CT system designs for oncology such as the Hitachi SceptreP3.

Patient couch

An important component of the combined system is the patient bed (or patient handling system, PHS) that must be compatible for both imaging modalities. PET/CT requires a redesign of the standard CT or PET couch for two reasons: the travel of the bed (stroke) has to be extended to accommodate the additional separation between the imaging fields, and the downward deflection of the bed from the weight of the patient has to be eliminated or at least minimized and corrected. The former is important to maximize the co-scan range—the imaging extent over which both CT and PET data can be acquired, while the latter is obviously essential to avoid an increasing and patient weight-dependent downward deflection of the bed as it moves through the gantry. Such a deflection would obviously limit the alignment accuracy. Novel solutions to these problems have been implemented by different vendors (Fig. 3).

CT-based attenuation correction (CT-AC)

For PET/CT a recognized strength is the availability of CT images for attenuation correction of the PET data [6, 7], eliminating the need for an additional, lengthy transmission scan. The use of the CT scanner to generate attenuation correction factors (ACFs) not only reduces the scan time by a significant amount but also results in more accurate ACFs. Since the attenuation values (μ) are energy dependent, the CT scan at a mean photon energy of about 70 keV must be scaled to PET (511 keV) energy. The mean energy of a polychromatic X-ray beam is defined as the energy of a monochromatic beam that would give the same linear attenuation as the polychromatic beam integrated over energy [8]. The polychromatic beam also results in beam hardening, the preferential interaction of lower energy photons as the beam traverses the body causing the mean energy to increase and the corresponding μ values to decrease.

The attenuation of X-rays by tissue depends on the density and the effective atomic number (Z_{eff}) of the material. At these energies, the physical processes by which X-rays are attenuated are the photoelectric effect and Compton scattering. The photoelectric probability varies approximately as Z_{eff}^4 and scales as $1/E^3$ with photon energy (E). The Compton scattering probability has little dependence on Z_{eff} and decreases linearly with 1/E. The linear attenuation coefficient for a given material is expressed by the sum of the two components:

$$\mu(E) = \rho_e\{\sigma_c(E) + \sigma_{ph}(E, Z_{eff})\}$$

where ρ_e is the electron density and σ_{ph} and σ_c are the photoelectric and Compton cross sections per electron, respectively. However at photon energies above about 100 keV in tissue, the photoelectric contribution is essentially negligible compared with the Compton contri-

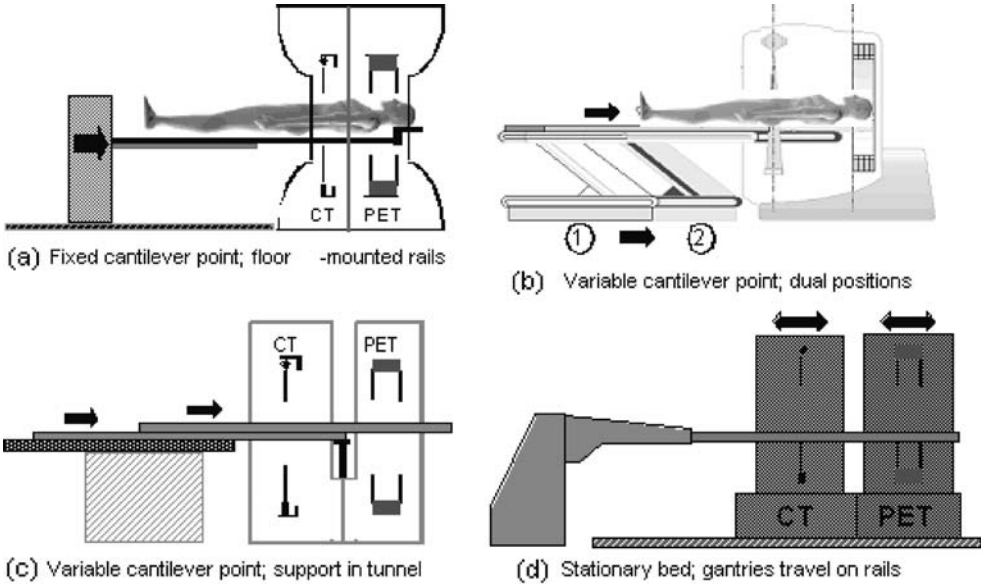

Fig. 3 Four different solutions to the patient handling system (PHS) that eliminate variable vertical deflection of the pallet as it advances into the tunnel of the scanner. The designs include (**a**) a bed with a fixed cantilever point where the entire couch assembly moves on floor-mounted rails, (**b**) a dual position bed with one position for CT and one for PET, (**c**) a patient couch that incorporates a support throughout the tunnel, and (**d**) a fixed couch with the gantry traveling on floor-mounted rails

bution and therefore the expressions for the attenuation coefficient at X-ray energy E_x and gamma energy E_γ are:

$$\mu(E_x) = \rho_e\{\sigma_c(E_x) + \sigma_{ph}(E_x, Z_{eff})\}$$
$$\mu(E_\gamma) = \rho_e\sigma_c(E_\gamma)$$

As a consequence of the two separate contributions to $\mu(E_x)$, a single measurement of $\mu(E_x)$ will not uniquely determine $\mu(E_\gamma)$, because, for example, an increase in Z_{eff} could offset a decrease in ρ_e resulting in no change in $\mu(E_x)$. In general, therefore, a simple energy scaling of $\mu(E_x)$ is insufficient to yield $\mu(E_\gamma)$. By restricting the problem to biological tissues for which Z_{eff} are all fairly comparable and noting that the contribution from σ_{ph} is relatively small even at X-ray energies, changes in $\mu(E_x)$ are primarily due to changes in tissue electron density. Thus, for the limited range of biological tissues, a single scaling factor can be used to convert $\mu(E_x)$ to $\mu(E_\gamma)$ for lung, liver, fat, muscle and other soft tissues. For spongiosa and cortical bone, however, the same scale factor will not apply because of the significant calcium and phosphorus content of bone tissue that result in Z_{eff} different from other tissues.

This issue has been addressed [6] by segmenting bone from soft tissue at a specific threshold and applying different scale factors to the two different tissue classifications—bone and non-bone corresponding to different values of Z_{eff}. Kinahan et al. adopted a threshold of 300 HU [6]. Subsequently Watson et al [8] proposed a mixture model in which all tissues with $\mu < \mu(\text{water})$ are treated as a mixture of air and water at various concentrations (k), while tissues with $\mu > \mu(\text{water})$ are treated as a mixture of water and cortical bone. Since this approach limits the composition to a single value for a given $\mu(E_x)$, a bilinear scaling function can be defined for biological tissues, as shown in Fig. 4. Recent publications on CT-AC for PET also propose a break-point at 0 HU (μ value for water) [9] although the most appropriate choice may be slightly greater than zero because some soft tissues and blood conform to the air-water mix but with densities greater than water for which a break-point around 60 HU is more appropriate.

The calibration function has been derived from phantom measurements and has also been validated with patient data [10]. A calibration of the CT ensures that the soft tissue values (μ<60 HU) are independent of the kVp setting of the X-ray tube. This independence does not apply to bone-like tissue with μ>60 HU and therefore different lines (slopes) are required for each kVp setting [11].

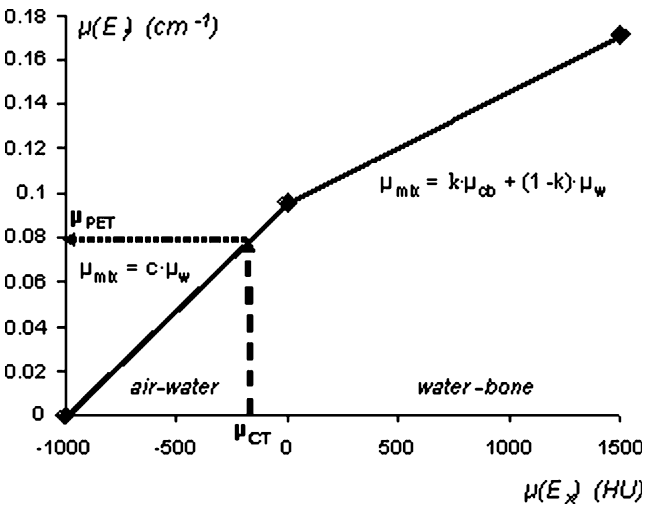

Fig. 4 The bilinear scaling function used to convert CT numbers (Hounsfield units) to linear attenuation values at 511 keV. The ACFs are generated by reprojecting the μ-map at 511 keV (*w* water, *cb* cortical bone, *k* concentration of the components of the mixture)

The CT data are acquired before the emission data so the ACFs can be generated for the entire volume. The CT images at about 70 keV are resampled to the spatial resolution of the emission data. The images are then scaled voxel-by-voxel to the energy of the emission data by applying the bilinear scaling function (Fig. 4). The scaled CT images are then forward projected to generate ACFs that match the sampling of the emission data. Since the introduction of PET/CT, CT-AC has been a significant focus of research to address the various possible artifacts.

Current emphasis in PET instrumentation

This section summarizes the current emphasis on improvements in the performance of the PET components of PET/CT systems.

Improved signal-to-noise with time-of-flight

The availability of fast scintillators with high stopping power such as LSO (and LYSO) has revived interest in PET time-of-flight (TOF) [12], interest that has been further stimulated by the announcement of the first commercial PET/CT system with TOF—the Philips Gemini TrueFlight (TF) [13]. Siemens has also recently reported clinical results for a series of over 100 patients scanned on a prototype PET/CT device with TOF capabilities [14]. The principle of TOF PET is illustrated schematically in Fig. 5; positron annihilation occurs in the patient at a distance $d+d_1$ from one detector and $d-d_1$ from the other detector. For photons traveling at the speed of light (c), the arrival time difference between the two photons at the detectors is $2d_1/c$. Photons originating from the center of the field of view (FOV) ($d_1=0$) obviously arrive in the detectors at the same time. PET systems with fast scintillators and electronics can measure this time difference to within a certain resolution. For example, for a coincidence timing resolution of 500 ps, the spatial uncertainty on the position of the annihilation is 7.5 cm. This uncertainty is not sufficient to place the annihilation within a 2-mm voxel (and thereby eliminate reconstruction) but it is superior to having no timing information at all and assigning equal probability to all voxels along the line-of-response (Fig. 5a). Instead, the most probable location of the annihilation is at the center of the uncertainty distribution in Fig. 5b. The TOF information is incorporated directly into the reconstruction algorithm leading to an improvement in signal-to-noise (SNR). The increase in SNR is proportional to $\sqrt{(D/\delta d)}$, where D is the diameter of the activity distribution and δd is the spatial uncertainty. For a 40-cm diameter uniform distribution and a 7.5 cm uncertainty, the increase in SNR is a factor of about 2.3. As the TOF resolution improves, the spatial uncertainty decreases and the SNR increases by a larger factor. TOF PET was first exploited in the early 1980s [12] with scintillators that were fast but did not have good stopping power for 511 keV photons. Interest declined until the recent emergence of scintillators that are both fast and sensitive. The new TOF PET systems based on LSO or LYSO must demonstrate good timing resolution that is stable over time so as to avoid frequent detector recalibration. While promising, the clinical impact of TOF PET has yet to be established. The published contributions to TOF development have been reviewed in more detail in [15].

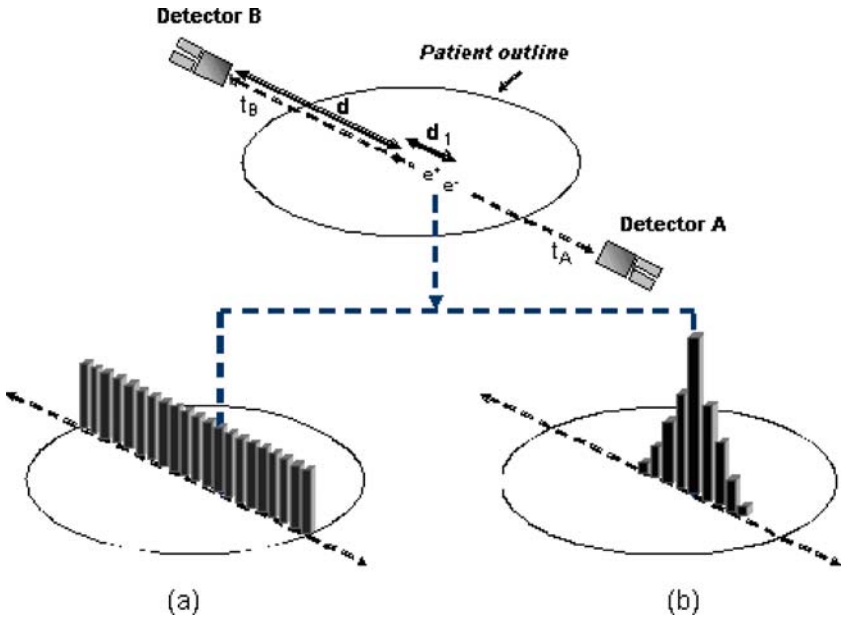

Fig. 5 Schematic illustrating PET data acquisition with the incorporation of TOF reconstruction. By measuring the time difference between the arrival of the two annihilation photons, the position of the positron annihilation along the line-of-response can be localized with an accuracy dependent on the precision of the temporal measurement: (**a**) without TOF information, the annihilation is located with equal probability along the line-of-response, and (**b**) using TOF information the annihilation point can be localized to a limited range, e.g., a 500 ps timing resolution corresponds to 7.5 cm FWHM

Improved sensitivity with increased axial FOV

The sensitivity of a PET system can be improved by the addition of more detector material. Planar sensitivity can be increased by extending the thickness of the scintillator. For example, a 50% increase in thickness of an LSO detector (20 mm to 30 mm) results in a 40% increase in sensitivity. However, increasing the axial extent of a PET scanner by 30% will result in a 78% increase in volume sensitivity (for 3-D acquisition with no septa). The latter thus makes more efficient use of the increased volume of LSO although there will also be an increase in the number of phototubes required (and hence increased cost). Following an injection of a radioactive tracer such as FDG, the patient receives a radiation dose from all annihilation photons, not just those emitted within the imaging FOV. Therefore, the greater the axial coverage, the better use is made of the emitted radiation and the more efficient use is made of a given volume of scintillator. For most PET/CT systems, axial PET coverage is about 16 cm, with one design having an axial extent of 18 cm [13]. The most recent design to be announced has an extended FOV covering 21.8 cm axially [16, 17].

Improved system model with PSF reconstruction

There has been significant progress during the past few years in image reconstruction methods through the introduction of statistically-based algorithms into the clinical setting. Previously, one of the earliest and most widely used 3-D reconstruction methods was the reprojection algorithm (3DRP) based on a 3-D extension of standard 2-D filtered back-projection [18]. While this algorithm works well for the lower noise environment of the brain, the quality for whole-body imaging is less than optimal, particularly when rod source ACFs are applied to low-count emission data. Fig. 6a shows a coronal image of a patient with a body mass index of 35 kg/m^2 reconstructed using 3DRP. Since CT-based ACFs have been applied the quality is probably better than would have been obtained with rod source ACFs. The development of Fourier rebinning (FORE) [19] was a breakthrough that enabled 3-D datasets to be accurately rebinned into 2-D datasets and then reconstructed in 2-D with a statistically-based expectation-maximization (EM) algorithm. However, it was not until the accelerated convergence achieved by the ordered-subset EM (OSEM) algorithm [20] that iterative methods became of clinical interest. While FORE and OSEM offer improved image quality compared with 3DRP, the incorporation of attenuation-based weights (AWOSEM) as suggested in the original paper by Hudson and Larkin, further improves image quality. This is demonstrated in Fig. 6b where the same dataset as in Fig. 6a has been reconstructed with FORE and AWOSEM [21]. Further improvement has been achieved by eliminating the rebinning step and implementing OSEM fully in 3-D with corrections for randoms, scatter and attenuation incorporated into the system model [22, 23].

In a recent development termed high-definition (HD) PET, the detector spatial response function has also been included in the reconstruction model [24]. The point spread function (PSF) varies throughout the FOV owing to the oblique penetration of the detectors by annihilation photons. By measuring this variability and then modeling the PSF, improved and near-uniform spatial resolution can be achieved throughout the FOV; the improvement can be seen by comparing Fig. 6b with the PSF reconstruction in Fig. 6c. Finally, in Fig. 6d both PSF and TOF have been incorporated into the reconstruction and the improved image quality can be seen by comparing this image with Fig. 6c; the PSF and PSF+TOF reconstructions are unsmoothed.

Motion-free PET/CT

Another area in PET/CT imaging that has recently received lots of interest is the reduction of image blurring due to object motion during PET data acquisition. One of the advantages of PET imaging is its ability to accurately quantify the radioactivity distribution in an area of interest. However, since the acquisition of PET data is not instantaneous (usually requiring 2–7 min per FOV depending on the imaging protocol) involuntary motion such as breathing or heart beating during data acquisition tends to blur internal targets thereby leading to inaccurately quantifiable images. This process can be seen in Fig. 7 where a set of six spheres were imaged while being moved in a sinusoidal manner to simulate breathing motion. The peak to peak motion distance was 2 cm and the period of motion was 5 s. Figure 7 clearly shows that the spheres no longer retain their shape but appear as ellipsoids due to the motion blur; furthermore, the apparent activity concentration in these ellipsoids is lower than in their corresponding original motion-free state.

One method to reduce motion blurring and restore activity concentration is to acquire the PET data in gated or list mode with retro- or prospective binning both of which are known as 4-D PET imaging. In both of these modes, the final result is a set of motion-free PET images that corresponds to the different segments of the motion cycle. Each image, however, is characterized by a low SNR due to the reduced counting statistic in each segment (bin). One approach to improve the image quality of each bin is to proportionally extend the overall data acquisition process so that the image quality of each bin is equivalent to that obtained without any object motion. This approach, however, raises practical difficulties related to patient discomfort and immobilization as well as to diminishing radioactivity concentration from decay and biological elimination [25]. In any case, however, it is postulated that

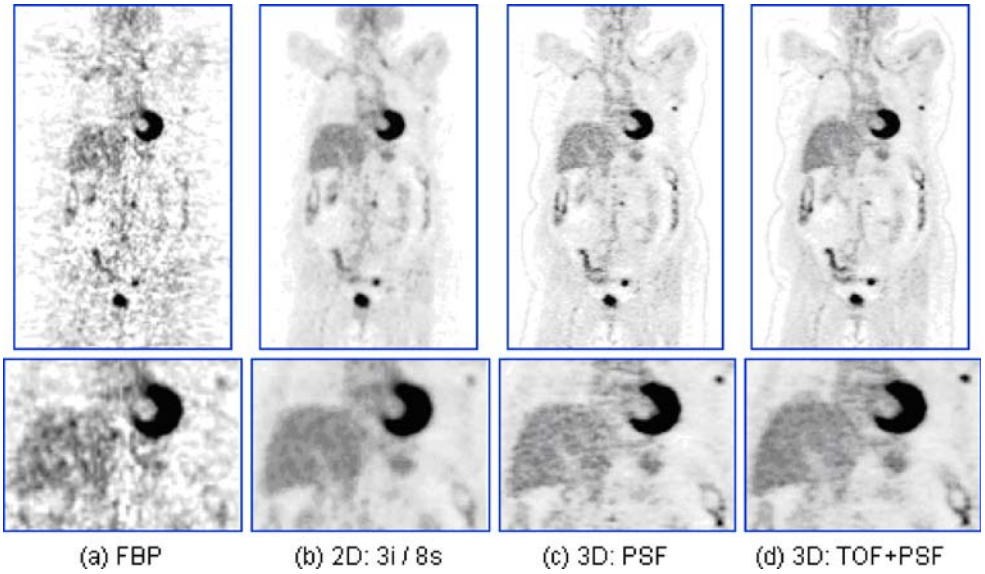

Fig. 6 Coronal section of an FDG-PET whole-body scan of a patient with a BMI of 35 kg/m^2 acquired in 3-D mode with septa retracted and reconstructed using: (**a**) 3-D filtered back-projection algorithm with reprojection (7 mm Gaussian smooth), (**b**) clinical reconstruction, FORE rebinning + 2-D OSEM (8 subsets, 3 iterations; 5 mm smoothing filter), (**c**) 3-D ordinary Poisson (OP) OSEM with PSF reconstruction (14 subsets, 2 iterations; no smoothing), and (**d**) 3-D OP-OSEM with both PSF and TOF reconstruction (14 subsets, 2 iterations, no smoothing)

with motion-free PET data acquisition, a new class of small low-contrasting lesions located in areas affected by breathing and cardiac motion would now be visible that otherwise would have been missed due to motion blur. This suggestion is made under the assumption that each of the gated PET image sets is accurately attenuation corrected using a matched CT dataset on a bin-by-bin basis throughout the motion cycle; the whole process is known as 4-D PET/CT imaging.

Several investigators have recently demonstrated the advantages of reducing motion blur on the quantitative accuracy of activity concentrations in PET imaging and have developed methods for reassembling the multiple low SNR images into a single image with improved SNR [26–41]. A relatively novel approach that has been recently introduced that does not require a gated mode of acquisition but reduces motion blur is the deep inspiration breath hold (DIBH) technique [42–44]. In this approach, a PET and a corresponding CT dataset are acquired during a specific segment. However, due to the limited time that patients can hold their breath at that motion phase, the process is repeated multiple times until the cumulative data acquisition period is equivalent to that utilized in PET imaging of a stationary object (about 3–5 min). Potential advantages of DIBH include the improvement in the probability of finding small lesions on CT images due to the filling of the lungs, the decrease in the amount of mismatch between the PET and CT images since they are acquired at the same phase, and the suppression of motion blur during PET data acquisition. These advantages come at the cost of increasing the total scan duration and requesting the patients to hold their breath at an unnatural phase for a relatively long period.

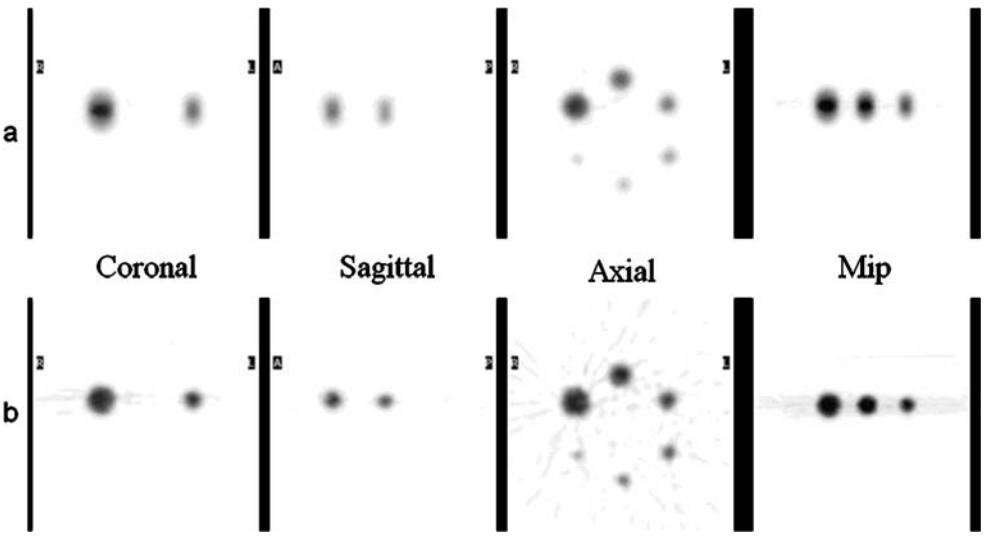

Fig. 7 PET images of a phantom with a set of six spheres of different diameters imaged while being moved in a sinusoidal manner to simulate breathing motion. The top images (**a**) clearly show that the spheres no longer retain their shape but appear as ellipsoids due to motion blur; furthermore, the apparent activity concentration in these ellipsoids is lower than in their corresponding original motion-free state shown in the bottom images (**b**)

Outstanding issues for application of PET/CT

The wide acceptance of PET/CT imaging in diagnostic radiology and radiation oncology is largely due to the ability of this imaging modality to improve patient diagnosis and treatment management. There are, however, several challenges of PET/CT imaging that are gaining prominence such as partial volume averaging, lesion segmentation, processing speed, and protocol workflows. These challenges should be mitigated in order for the acceptance of PET/CT imaging in the clinical assessment and management of patients to continue as well as increase.

Partial volume effect

Partial volume averaging (PV) is the underestimation of activity concentration in a lesion due to the limited spatial resolution of PET. PV mostly affects lesions of sizes less than 2.5 to 3.0 times the PET resolution. However, any sharp edges of an object (even if the object is bigger than three times the PET resolution) are also affected by PV and are blurred on in the reconstructed image. Since one of the main advantages of PET imaging is its ability to detect and quantify the activity concentration in small lesions, PV becomes one of the major factors that hinder the accomplishment of this objective. Lesions that have a decreased activity concentration following therapy cannot be confirmed based on PET imaging alone if this decrease is due to a response to therapy or actually a decrease in lesion size, which resulted in PV and hence a decrease in measured activity concentration. There are several factors that affect the severity of PV other than lesion size such as the shape of the lesion, the lesion to background activity concentration, and the reconstruction algorithm and parameters used to generate the final PET images. These additional factors, although important, have less impact on the final quantitative value than lesion size, particularly when the spatial resolution of the PET system is relatively low. Current commercially available PET systems have spatial resolutions on the order of 4–7 mm, with which PV effects start to occur in lesions as large as 1.2–2 cm. The additional factors affecting the severity of PV can increase this range to 2.5–3.5 cm. Improving the PET image spatial resolution by modeling the detector blurring function during image reconstruction (section Motion-free PET/CT above) reduces the effects of PV and hence improves the accuracy of determining the actual activity concentration in small lesions.

Several methods have been proposed to mitigate the effects of PV with different levels of success. These methods have been summarized in a recent report by Soret et al. [45]. In any case, none of these approaches is currently used in routine clinical settings since none has been implemented by any of the PET/CT system manufacturers on their respective systems and hence the accurate determination of lesion activity concentration remains a persistent challenge in PET imaging.

Lesion segmentation

One of the differentiating attributes of PET images is their blurry appearance due to the limited spatial resolution of this imaging modality. This aspect limits the ability to accurately delineate the actual boundaries of lesions and hence affects the usefulness of PET images for treatment planning. This impediment has large ramifications on the widespread use and acceptance of PET imaging in radiation oncology applications. Traditionally, lesion volumes were determined from PET images using subjective contrast settings based on the physician's preference. This approach, however, results in large interobserver variability and necessitates a standardized approach to lesion segmentation. The process of delineating tumor volumes on PET images is also further complicated by PV effects (described above) since the apparent lesion boundaries on the reconstructed PET image depend on the same factors that affect PV such as lesion size, lesion to background ratio and reconstruction parameters.

Several methods have been proposed to segment lesion volumes from PET images. Some of these approaches depend on selecting a fixed threshold setting while others rely on derived functional forms that relate the threshold setting to the mean activity concentration in the lesion and the background level [46–54]. In all cases, these threshold settings fail when applied to small lesion volumes due to PV effects. At the present time there is no method that has gained wide acceptance for segmenting tumor volumes from PET images although a 40–50% fixed threshold of the maximum activity concentration in a lesion remains to be utilized in many settings and is now available as an option on some PET data analysis workstations. This approach, however, should be used with caution when applied to small lesions since it will overestimate the true lesion volume due to PV.

The difficulty in approximating the true lesion volume from PET images is further exacerbated by other confounding factors such as lesion motion during PET data acquisition which will reduce the apparent activity concentration in a lesion. Another important factor is the inaccuracy in attenuation correction due to the mismatch between the PET and CT images, which will also lead to a discrepancy between the actual and apparent activity concentration in a lesion [55, 56]. Based on these challenges, there has been a continued interest among different investigators and research centers to develop new approaches and algorithms towards resolving this issue.

These interests have been largely fueled by the potential advantages gained from utilizing PET tumor volumes for radiation treatment planning purposes and their possible impact on patient management.

Reconstruction timing and protocol workflows

The time required to generate the final PET images from a PET/CT examination is starting to represent a challenge to the productivity and throughput of this imaging modality. This issue is primarily due to the combined effects of several confounding factors. The current trend of acquiring PET data in 3-D rather than 2-D mode, as demonstrated by the introduction of 3-D-only systems, has resulted in an increase in the allowable coincidence events, which ultimately is reflected in an increase in reconstruction time to generate the final PET images. Furthermore, the recent introduction of advanced full 3-D image reconstruction algorithms that incorporate various correction models during their optimization process has also added to the challenge of keeping the reconstruction time as short as possible. In addition, as PET systems continue to be more sensitive and efficient and the acquisition duration per bed position continues to decrease (currently between 1 min and 7 min per FOV), the requirement to generate the final image set in a short time period following the data acquisition becomes more difficult. Also, the recommendation to generate nonattenuation-corrected PET images to resolve potential artifacts generated by the CT-based attenuation correction [57] further increases the necessary time to generate the final images. Finally, TOF-PET also adds to the complexity of the reconstruction algorithm and the time required to generate the final images since each coincidence event requires additional information pertaining to its detection time. All of these factors contribute to increasing the time to generate the final PET images. This aspect represents an emerging area of active research interest, and in particularly TOF imaging and its associated image processing requirement is starting to gain importance within the PET imaging community [58–61].

Another area that represents a prospect for the increased utilization of PET/CT in clinical applications is the introduction of optimized protocol workflows that integrate the correction schemes that have been proposed to resolve some of the challenges of this imaging modality, such as the effects of mismatch between PET and CT images as well as the effects of lesion motion and lesion segmentation. These workflows should be designed with the objective of ease of use and prompt generation of the final images with minimal user interaction. Currently, none of the PET/CT system manufacturers provide optimized workflows on their system platforms. Ultimately, the development of such protocols will facilitate the use of the system capabilities to their fullest and help in evaluating the impact of the suggested correction schemes on patient management.

Clinical applications of PET/CT

Diagnosis and staging in oncology

The use of PET and more recently PET/CT imaging in diagnostic radiology spans the fields of cardiology, neurology, and oncology. However, based on the clinical indications that are approved by the Centers for Medicare and Medicaid services (CMS) for this imaging modality, the majority of PET/CT imaging is performed in oncology evaluation—namely staging and restaging of cancer. Several publications have shown that PET/CT imaging is better than PET or CT alone for staging and restaging in a variety of cancers [62–64]. This conclusion was predominantly based on showing a significant improvement in specificity and to some extent in sensitivity with the resultant improvement in accuracy shown to be statistically significant and on average ranging between 10% and 15% [63]. The improvements in accuracy coupled with the convenience of presenting morphological and biological information to physicians have rendered PET/CT imaging as the most important cancer imaging modality at the present time [63]. For cancer indications that are not covered by CMS, a recent study by Hillner et al. [65] evaluating the impact of PET/CT imaging on patient management through the national oncologic PET registry (NOPR) showed that overall, physicians changed their intended management in 36.5% (95% CI, 35.9 to 37.2) of cases following PET/CT imaging.

Therapy planning

The advent of conformal radiation therapy and intensity-modulated radiation therapy necessitates more precise target volume definitions for dose-sparing of normal tissues. Traditionally, CT has been the modality of choice for radiation therapy planning (RTP) of these treatment techniques. However, CT has been shown to have a relatively low sensitivity and specificity for detecting tumor tissue [66]. PET and more recently PET/CT imaging on the other hand, have been shown to have higher values for both of these metrics [67]. In a meta analysis [67] for solid tumors, PET/CT imaging was shown to have a sensitivity of 92% and a specificity of 93% compared to 85% and 88% for PET and 64% and 83% for CT alone, respectively. In this regard, it is not surprising that PET/CT imaging rather than CT or PET alone has been suggested as a primary tool to facilitate RTP [68]. In addition, PET/CT provides

knowledge about the morphology as well as the biology of the tumor. Tumor biology has been identified as an essential factor for effective dose delivery [69]. With PET/CT imaging the biological tumor volume [69] allows the radiation dose to be modulated according to the distribution of the PET signal intensity within the tumor volume, thereby resulting in more efficient and effective delivery of radiation dose to the tumor while sparing the surrounding healthy tissue [69, 70]. Also, the requirement for highly precise and reproducible patient positioning during the imaging and treatment sessions to ensure accurate tumor delineation and effective dose delivery enforces the choice of a combined PET/CT system over stand-alone PET and CT systems [71]. The collective effects of these three factors render PET/CT imaging an obvious choice for RTP over other imaging modalities such as PET or CT alone.

To date, the majority of PET/CT applications for RTP purposes are in the thorax. A recent review on PET/CT utilization for radiotherapy planning in lung cancer showed differences in the range 30% to 60% between PET-derived contours versus CT-only target volumes [72]. Obviously, what constitutes a significant alteration of the plan is a matter of debate. Many studies indicate a change in volume of ≥25% as significant [73, 74]. However, an issue that deserves to be addressed in more detail is the nature of the change in the gross tumor volume in terms of primary tumor and nodal target volumes [66].

An important but controversial issue concerning the use of PET imaging for RTP purposes is the threshold selection of the PET images when contouring the tumor volume. This issue is discussed in section Lesion segmentation above but currently represents one of the main obstacles for the wide adoption of PET imaging in RTP. It is anticipated that, with the development of new approaches for accurate target volume delineation, the use of PET and PET/CT imaging will become the standard for RTP.

Future developments in PET/CT

There have been several advances in PET/CT system design and their capabilities since this combined imaging modality was first introduced in 2001. However, although PET/CT imaging has seen significant improvements over the past few years, there still exist a number of opportunities to improve the performance of this imaging modality that would further solidify its acceptance as the modality of choice in a wide range of applications. These improvements lie primarily in volume sensitivity and spatial resolution as well as in the development of new radiopharmaceuticals that provide comprehensive in situ functional characterization of cancer to guide individualized therapy.

Improvements in sensitivity

The sensitivity of a PET system is limited by its intrinsic as well as its geometric efficiencies. Methods to improve the intrinsic efficiency rely on using detectors with high stopping power and/or increasing the depth of the detector, as discussed in section Improved sensitivity with increased axial FOV above. However, current PET use detectors such as BGO, LYSO, and LSO that are 20–30 mm in depth and already capable of stopping 70–90% of the annihilation photons [75]. So any further improvement in the detector intrinsic efficiency would not have a large impact on the volume sensitivity. This situation, however, is reversed for the geometric efficiency of the system, which can be optimized by extending the axial FOV. Townsend [76] has shown that by increasing the FOV from 16.2 cm to 21.8 cm the system sensitivity increases by 78%, albeit at a possible increase in cost due to the additional hardware required. Further increasing the axial extent of the PET to cover the whole body will also increase the total system sensitivity as well as reduce total scan duration, patient motion and, as a consequence, image blurring. Several PET system designs with increased axial extent have already been proposed [77–79]. Some of these designs effectively cover the majority of the body in a single bed position. The proposed advantages of such designs other than higher sensitivity and shorter scan durations are lower injected dose, which also translates to lower costs, and the possibility to facilitate radionuclide biodistribution studies over the whole body.

Improvements in PET sensitivity by increasing the axial FOV can be coupled with TOF scanner designs to produce an effective improvement in SNR that is roughly one order of magnitude higher than in current systems [75]. This improvement in SNR has a direct effect on producing PET images with high spatial resolution. However, as mentioned above, increasing the axial FOV of the PET will result in an increase in the overall cost of the scanner. Methods to reduce the overall cost can include reducing the total number of photomultiplier tubes through the use of a quadrant sharing design, replacing the photomultiplier tube with avalanche photodiode detectors (APDs), or development of cheaper detectors. Other drawbacks of increasing the axial FOV are increased dead-time and the need for a sophisticated normalization correction scheme and reconstruction algorithms.

Improvements in spatial resolution

PET images are characterized by low spatial resolution. This drawback is mainly due to four factors: detector size, positron range, acolinearity of the annihilation photos, and depth of interaction (DOI) which results in a nonstationary resolution across the transverse FOV. Improving PET image

resolution potentially has a large impact on the wide acceptance of this imaging modality in RTP and its ability to accurately quantify the response to therapy, both of which are expected to become major applications of PET imaging in the future. Furthermore, the low PET resolution results in PV, which limits the ability to accurately quantify treatment response (see section Partial volume effect above). Methods to improve image resolution depend on mitigating the four factors that affect image resolution. This can be achieved by modeling the effects of each of these components during the image reconstruction process. Recently, one manufacturer (Siemens Medical Solutions) did just that for the effect of detector size during image reconstruction to minimize the impact of this factor [24]. Similarly, the effects of positron range could also be modeled depending on the radionuclide that is being used. For ^{18}F the effect of positron range is relatively small since the root mean square of the positron range in water for ^{18}F is 0.2 mm [80]. That is not the case for other radionuclides such as ^{82}Rb, which is used in cardiac imaging and has a range of 2.6 mm. Positron range is currently not corrected for on any PET system.

The effect of acolinearity is probably one of the most important factors that affect image resolution in clinical PET. This factor is proportional to the detector ring diameter and is of the order of 2.2 mm for a PET system with a 100-cm ring diameter. Since the current trend is to increase the bore diameter to accommodate large patients as well as those that should be imaged in the treatment position, care should be taken not to increase the ring diameter further. Currently there are no models that correct for acolinearity that are available on any commercial or research PET system. However, such an approach could greatly improve the effective resolution of PET images.

Finally, the effect of DOI largely prevails in preclinical systems due to the curvature of the detector ring at small radial distances from the center of the FOV. In clinical systems, DOI effects occur at larger distances from the center of the FOV. Current clinical systems have spatial resolutions that vary about 1–2 mm at distances of 20–30 mm from the center of the FOV. Methods to mitigate the effects of DOI rely on phoswitch detectors [81, 82] that can determine the DOI of a photon in a detector. Currently there exists one commercial clinical PET system (HRRT, Siemens Medical Solutions) with phoswitch detectors, but that system is for brain imaging only [83].

New drug development

In addition to improving the physical characteristics of the PET components, the development and adoption of new positron-emitting radiopharmaceuticals will have a profound impact on solidifying the reliance on PET imaging as the modality of choice for functional investigation at the molecular level. It is important to note that the current prominence of PET imaging is based on a single radiopharmaceutical—^{18}F-FDG—an analog for imaging glucose metabolism (other radiopharmaceuticals such as ammonia and rubidium are used in cardiology, but they constitute a relatively small proportion of the overall clinical use of PET imaging); therefore, it is expected that with the introduction of other positron-emitting radiopharmaceuticals PET imaging will gain even more prominence in oncology, neurology and cardiology. One of the main advantages of PET imaging is its ability to image a functional process at its molecular level (hence molecular imaging) while using a trace amount (nano- to picomoles) of a radiopharmaceutical that is specifically designed for the process in question. This can be achieved by using radiopharmaceuticals with high specific activity (amount of radioactive material per unit mass of material) in order to detect the radiotracer without perturbing the underlying process. This capability coupled with the ability of PET/CT to accurately quantify the underlying functional process as well as its anatomical layout signifies the uniqueness of this imaging modality

Several radionuclides have been investigated as potential radiolabels for different radiotracers in PET imaging [84–87]. The consensus, however, is that ^{18}F is the optimum choice among other possible candidates such as ^{11}C, ^{13}N, and ^{68}Ga. The advantages of ^{18}F are mainly its wide availability, automated synthesis, relatively long half-life allowing its transport, short positron range, acceptable radiation dosimetry, high production and labeling yields, and high specific activity. Based on these attributes and fueled by the emergence of PET imaging as the modality of choice for molecular investigation, there has been a series of new ^{18}F-labeled tracers that have been developed or are currently under development, the majority of which are specific to oncology. A recent survey of these tracers can be found elsewhere [88, 89]. These tracers promise to broaden the ability of PET/CT imaging to provide comprehensive in situ functional characterization of cancer to guide individualized therapy.

The future possibility of accurate localization and comprehensive functional phenotyping of tumors with multitracer PET/CT imaging is, therefore, very real. However, issues of tangible downstream treatment impact and cost-effectiveness, which remain unresolved for FDG-PET/CT will be no less (and perhaps more) critical and challenging for newer PET tracers. It is hoped, however, that lessons learned from the validation of FDG-PET/CT imaging in the clinic can streamline this process for future PET tracers.

From PET/CT to PET/MRI

The development of PET/MRI is obviously technically more challenging than PET/CT because phototubes are sensitive even to low magnetic fields. Also, MRI demands very high field homogeneity and the presence of PET detectors within the field could potentially interfere with the MR imaging. In contrast, the PET detectors have to withstand not only a high static field level but also the rapidly changing field gradients required by the imaging process.

Christensen et al. were one of the first groups to address some of these issues in the mid 1990s [90]. Their design was based on placing PET detectors inside a clinical MR scanner and extracting the information from the scintillator over light guides that transported the signals to phototubes positioned outside the magnetic field. The first simultaneous acquisition of FDG uptake data and MR spectroscopy in an isolated, perfused rat heart model was reported in 1996 [91]. The device used was a novel gamma photon detector operated inside a 9.4-T MR spectrometer. At around the same time as this work, Shao et al. developed a small ring of PET detectors for preclinical small-animal imaging [92]. A second, larger prototype was built with a ring diameter of 5.6 cm that simultaneously acquired MR and PET data in small animals using a number of different pulse sequences [93].

More recently, the focus of PET/MRI development for preclinical imaging has been on the use of APDs as photodetectors owing to their insensitivity to magnetic fields [94, 95]. The combination of scintillator and APD can function within a high magnetic field (up to 9.4-T) and tolerate the changing field gradients [96, 97]; in addition, the detectors do not interfere with the operation of the MRI scanner. Recently, a brain-only PET detector ring has been developed based on LSO blocks and APDs [98, 99] that can be inserted into a 3-T MRI scanner. The combined system has successfully acquired simultaneously FDG-PET data and MR data including proton spectroscopy and echo planar gradient-echo sequences [100]. In contrast to PET/CT where the two modalities are acquired sequentially, the PET/MRI brain insert allows the modalities to acquire data simultaneously, potentially opening up new research applications for neuroscience. However, the attenuation correction of the PET data is not as straightforward for PET/MRI as for PET/CT because the MR signal is not a measure of the electron density in the tissue. This is evident from the fact that air and bone give essentially the same MR signal whereas they have very different linear attenuation values. Strategies are currently being developed to address the issue of MR-based PET attenuation correction [101, 102].

The question as to whether PET/MRI will supplant or replace PET/CT in the clinic is a topic of considerable debate at the present time. While there have been some suggestions that PET/MRI could replace PET/CT [103], it does not seem very likely that the addition of a PET insert to an MRI system will attract clinical applications away from PET/CT. Both modalities, CT and MRI, have well-recognized strengths especially for imaging malignant disease, and this is unlikely to change as a consequence of the availability of an MR-compatible PET insert. Hopefully, the contents of this timely supplement on PET/MRI may help, at least to clarify and broaden, if not to resolve, this ongoing debate.

Conflicts of interest D. W. Townsend is a consultant for Siemens Molecular Imaging. O. Mawlawi has no conflicts of interest.

References

1. Beyer T, Townsend DW, Brun T, Kinahan PE, Charron M, Roddy R, et al. A combined PET/CT scanner for clinical oncology. J Nucl Med 2000;41:1369–79.
2. Charron M, Beyer T, Bohnen NN, Kinahan PE, Dachille M, Jerin J, et al. Image analysis in patients with cancer studied with a combined PET and CT scanner. Clin Nucl Med 2000;25:905–10.
3. Meltzer CC, Luketich JD, Friedman D, Charron M, Strollo D, Meehan M, et al. Whole-body FDG positron emission tomographic imaging for staging esophageal cancer comparison with computed tomography. Clin Nucl Med 2000;25:882–7.
4. Kluetz PG, Meltzer CC, Villemagne VL, Kinahan PE, Chander S, Martinelli MA, et al. Combined PET/CT imaging in oncology. Impact on patient management. Clin Positron Imaging 2000;3:223–30.
5. Townsend DW, Beyer T, Blodgett TM. PET/CT scanners: a hardware approach to image fusion. Semin Nucl Med 2003;33:193–204.
6. Kinahan PE, Townsend DW, Beyer T, Sashin D. Attenuation correction for a combined 3D PET/CT scanner. Med Phys 1998;25:2046–53.
7. Kinahan PE, Hasegawa BH, Beyer T. X-ray-based attenuation correction for positron emission tomography/computed tomography scanners. Semin Nucl Med 2003;33:166–79.
8. Watson CC, Townsend DW, Bendriem B. PET/CT systems. In: Aarsvold WAJ, editor. Emission tomography. London: Elsevier Science; 2004. p. 195–212.
9. Burger C, Goerres G, Schoenes S, Buck A, Lonn AH, Von Schulthess GK. PET attenuation coefficients from CT images: experimental evaluation of the transformation of CT into PET 511-keV attenuation coefficients. Eur J Nucl Med Mol Imaging 2002;29:922–7.
10. Watson CC, Rappoport V, Faul D, Townsend DW, Carney JP. A method for calibrating the CT-based attenuation correction of PET in human tissue. IEEE Trans Nucl Sci 2006;53:102–7.
11. Carney JP, Townsend DW. CT-based attenuation correction for PET/CT scanners. In: von Schulthess GK, editor. Clinical molecular anatomic imaging: PET-CT and SPECT-CT. Philadelphia: Lippincott Williams and Wilkins; 2006. p. 54–62.
12. Budinger TF. Time-of-flight positron emission tomography: status relative to conventional PET. J Nucl Med 1983;24:73–8.
13. Surti S, Kuhn A, Werner ME, Perkins AE, Kolthammer J, Karp JS. Performance of Philips Gemini TF PET/CT scanner with special consideration for its time-of-flight imaging capabilities. J Nucl Med 2007;48:471–80.

14. Conti M, Townsend DW, Casey M, Lois C, Jakoby BW, Long MJ, et al. Assessment of the clinical potential of a time-of-flight PET/CT scanner with less than 600 ps timing resolution. J Nucl Med 2008;49:411.
15. Muehllehner G, Karp JS. Positron emission tomography. Phys Med Biol 2006;51:R117–37.
16. Jakoby BW, Bercier Y, Watson CC, Rappoport V, Young J, Bendriem DW. Physical performance and clinical workflow of a new LSO HI-REZ PET/CT scanner. Nuclear Science Symposium Conference Record, 2006, IEEE, vol. 5, p 3130–4.
17. Townsend DW, Jakoby B, Long MJ, Carr C, Hubner K, Guglielmo C. Performance and clinical workflow of a new combined PET/CT scanner. J Nucl Med 2007;48:437.
18. Kinahan P, Rodgers JG. Analytic 3D image reconstruction using all detected events. IEEE Trans Nucl Sci 1989;36:964–8.
19. Defrise M, Kinahan PE, Townsend DW, Michel C, Sibomana M, Newport DF. Exact and approximate rebinning algorithms for 3-D PET data. IEEE Trans Med Imaging 1997;16:145–58.
20. Hudson HM, Larkin RS. Accelerated image reconstruction using ordered subsets of projection data. IEEE Trans Med Imaging 1994;13:601–9.
21. Comtat C, Kinahan P, Defrise M, Michel C, Townsend DW. Fast reconstruction of 3D PET data with accurate statistical modeling. IEEE Trans Nucl Sci 1998;45:1083–9.
22. Comtat C, Bataille F, Michel C, Jones JP, Sibomana M, Janeiro L, et al. OSEM-3D reconstruction strategies for the ECAT HRRT. Nuclear Science Symposium Conference Record, 2004, IEEE, vol. 6, p 3492–6.
23. Liu X, Comtat C, Michel C, Kinahan P, Defrise M, Townsend D. Comparison of 3-D reconstruction with 3D-OSEM and with FORE+OSEM for PET. IEEE Trans Med Imaging 2001;20:804–14.
24. Panin VY, Kehren F, Michel C, Casey M. Fully 3-D PET reconstruction with system matrix derived from point source measurements. IEEE Trans Med Imaging 2006;25:907–21.
25. de Juan R, Seifert B, Berthold T, von Schulthess GK, Goerres GW. Clinical evaluation of a breathing protocol for PET/CT. Eur Radiol 2004;14:1118–23.
26. Klein GJ, Reutter BW, Ho MH, Reed JH, Huesman RH. Real-time system for respiratory-cardiac gating in positron tomography. IEEE Trans Nucl Sci 1998;45:2139–43.
27. Nehmeh SA, Erdi YE, Ling CC, Rosenzweig KE, Schoder H, Larson SM, et al. Effect of respiratory gating on quantifying PET images of lung cancer. J Nucl Med 2002;43:876–81.
28. Nehmeh SA, Erdi YE, Rosenzweig KE, Schoder H, Larson SM, Squire OD, et al. Reduction of respiratory motion artifacts in PET imaging of lung cancer by respiratory correlated dynamic PET: methodology and comparison with respiratory gated PET. J Nucl Med 2003;44:1644–8.
29. Thorndyke B, Schreibmann E, Maxim P, Loo B, Boyer A, Koong A, et al. Enhancing 4D PET through retrospective stacking. Med Phys 2005;32:2094.
30. Klein GJ, Huesman RH. Four-dimensional processing of deformable cardiac PET data. Med Image Anal 2002;6:29–46.
31. Livieratos L, Stegger L, Bloomfield PM, Schafers K, Bailey DL, Camici PG. Rigid-body transformation of list-mode projection data for respiratory motion correction in cardiac PET. Phys Med Biol 2005;50:3313–22.
32. Lamare F, Cresson T, Savean J, Cheze Le Rest C, Reader AJ, Visvikis D. Respiratory motion correction for PET oncology applications using affine transformation of list mode data. Phys Med Biol 2007;52:121–40.
33. Lalush DS, Cui L, Tsui B. A priori motion models for four-dimensional reconstruction in gated cardiac SPECT. Nuclear Science Symposium Conference Record, 1996, IEEE, vol. 3.
34. Qi J, Huesmans RH. List mode reconstruction for PET with motion compensation: a simulation study. Proceedings Nuclear Symposium Biological Imaging Conference, 2002, p 413–6.
35. Gilland DR, Mair BA, Bowsher JE, Jaszczak RJ. Simulations reconstruction and motion estimation for gated cardiac ECT. IEEE Trans Nucl Sci 2002;49:2344–9.
36. Cao Z, GD R, Mair BA, Jaszczak RJ. Three-dimensional motion estimation with image reconstruction for gated cardiac. ECT IEEE Trans Nucl Sci. 2003;50:384–8.
37. Jacobson MW, Fessler JA. Joint estimation of image and deformation parameters in motion-correction PET. Nuclear Symposium and Medical Imaging Conference Record, 2004, IEEE, vol. 5, p 3290–4.
38. Rahmim A, Bloomfield P, Houle S, Lenox M, Michel C, Buckley KR, et al. Motion compensation in histogram-mode and list-mode EM reconstructions: beyond the event-driven approach. IEEE Trans Nucl Sci 2004;51:2588–96.
39. Gilland DR, Mair BA, Sun J. Joint 4D reconstruction and motion estimation in gated cardiac ECT. Proceedings of the Eighth International Meeting on Fully Three-Dimensional Image Reconstruction in Radiology and Nuclear Medicine, Salt Lake City, 6–9 July 2005. p 303–6.
40. Gravier E, Yang Y. Motion-compensated reconstruction of tomographic image sequences. IEEE Trans Nucl Sci 2005;51:51–6.
41. Qiao F, Pan T, Clark JW Jr, Mawlawi OR. A motion-incorporated reconstruction method for gated PET studies. Phys Med Biol 2006;51:3769–83.
42. Nehmeh SA, Erdi YE, Meirelles G, et al. Deep-inspiration breathhold PET/CTof the thorax. J Nucl Med 2006;48:22–6.
43. Meirelles G, Erdi YE, Nehmeh SA, et al. Deep-inspiration breathhold PET/CT: clinical findings with a new technique for detection and characterization of thoracic lesions. J Nucl Med 2006;48:712–9.
44. Kawano T, Ohtake E, Inoue T. Deep-inspiration breath hold PET/CT of lung cancer: maximum standardized uptake value analysis of 108 patients. J Nucl Med 2008;49:1223–31.
45. Soret M, Bacharach SL, Buvat I. Partial volume effect in PET tumor imaging. J Nucl Med 2007;48:932.
46. Mah K, Caldwell CB, Ung YC, Danjoux CE, Balogh JM, Ganguli SN, et al. The impact of (18)FDG-PET on target and critical organs in CT-based treatment planning of patients with poorly defined non-small-cell lung carcinoma: a prospective study. Int J Radiat Oncol Biol Phys 2002;52:339–50.
47. Nestle U, Walter K, Schmidt S, Licht N, Nieder C, Motaref B, et al. 18F-deoxyglucose positron emission tomography (FDG-PET) for the planning of radiotherapy in lung cancer: high impact in patients with atelectasis. Int J Radiat Oncol Biol Phys 1999;44:593–7.
48. Black QC, Grills IS, Kestin LL, Wong CY, Wong JW, Martinez AA, et al. Defining a radiotherapy target with positron emission tomography. Int J Radiat Oncol Biol Phys 2004;60:1272–82.
49. Biehl KJ, Kong FM, Dehdashti F, Jin JY, Mutic S, El Naqa I, et al. 18F-FDG PET definition of gross tumor volume for radiotherapy of non-small cell lung cancer: is a single standardized uptake value threshold approach appropriate? J Nucl Med 2006;47:1808–12.
50. Nestle U, Kremp S, Schaefer-Schuler A, Sebastian-Welsch C, Hellwig D, Rube C, et al. Comparison of different methods for delineation of 18F-FDG PET-positive tissue for target volume definition in radiotherapy of patients with non-small cell lung cancer. J Nucl Med 2005;46:1342–8.
51. Erdi YE, Mawlawi O, Larson SM, Imbriaco M, Yeung H, Finn R, et al. Segmentation of lung lesion volume by adaptive positron emission tomography image thresholding. Cancer 1997;80(12 Suppl):2505–9.

52. Daisne JF, Sibomana M, Bol A, Doumont T, Lonneux M, Gregoire V. Tri-dimensional automatic segmentation of PET volumes based on measured source-to-background ratios: influence of reconstruction algorithms. Radiother Oncol 2003;69:247–50.
53. Jentzen W, Freudenberg L, Eising EG, Heinze M, Brandau W, Bockisch A, et al. Segmentation of PET volumes by iterative image thresholding. J Nucl Med 2007;48:108–14.
54. Drever L, Roa W, McEwan A, Robinson D. Iterative threshold segmentation for PET target volume delineation. Med Phys 2007;34:1253–65.
55. Erdi YE, Nehmeh SA, Pan T, Pevsner A, Rosenzweig KE, Mageras G, et al. The CT motion quantitation of lung lesions and its impact on PET-measured SUVs. J Nucl Med 2004;45:1287–92.
56. Pan T, Mawlawi O, Nehmeh SA, Erdi YE, Luo D, Liu HH, et al. Attenuation correction of PET images with respiration-averaged CT images in PET/CT. J Nucl Med 2005;46:1481–7.
57. Delbeke D, Coleman RE, Guiberteau MJ, Brown ML, Royal HD, Siegel BA, et al. Procedure guideline for tumor imaging with 18F-FDG PET/CT 1.0. J Nucl Med 2006;47:885–95.
58. Defrise M, Casey ME, Michel C, Conti M. Fourier rebinning of time-of-flight PET data. Phys Med Biol 2005;50:2749–63.
59. Vandenberghe S, Daube-Witherspoon ME, Lewitt RM, Karp JS. Fast reconstruction of 3D time-of-flight PET data by axial rebinning and transverse mashing. Phys Med Biol 2006;51:1603–21.
60. Cho S, Li Q, Ahn S, Bai B, Leahy RM. Iterative image reconstruction using inverse fourier rebinning for fully 3-D PET. IEEE Trans Med Imaging 2007;26:347–58.
61. Kao CM. Windowed image reconstruction for time-of-flight positron emission tomography. Phys Med Biol 2008;53:3431–45.
62. Czernin J, Auerbach MA. Clinical PET/CT imaging: promises and misconceptions. Nuklearmedizin 2005;44(Suppl 1):S18–23.
63. Czernin J, Allen-Auerbach M, Schelbert HR. Improvements in cancer staging with PET/CT: literature-based evidence as of September 2006. J Nucl Med 2007;48(Suppl 1):78S–88S.
64. Weber WA, Grosu AL, Czernin J. Technology insight: advances in molecular imaging and an appraisal of PET/CT scanning. Nat Clin Pract Oncol 2008;5:160–70.
65. Hillner BE, Siegel BA, Liu D, Shields AF, Gareen IF, Hanna L, et al. Impact of positron emission tomography/computed tomography and positron emission tomography (PET) alone on expected management of patients with cancer: initial results from the National Oncologic PET Registry. J Clin Oncol 2008;26:2155–61.
66. Gregoire V, Haustermans K, Geets X, Roels S, Lonneux M. PET-based treatment planning in radiotherapy: a new standard? J Nucl Med 2007;48(Suppl 1):68S–77S.
67. Antoch G, Saoudi N, Kuehl H, Dahmen G, Mueller SP, Beyer T, et al. Accuracy of whole-body dual-modality fluorine-18-2-fluoro-2-deoxy-D-glucose positron emission tomography and computed tomography (FDG-PET/CT) for tumor staging in solid tumors: comparison with CT and PET. J Clin Oncol 2004;22:4357–68.
68. Ciernik IF, Dizendorf E, Baumert BG, Reiner B, Burger C, Davis JB, et al. Radiation treatment planning with an integrated positron emission and computer tomography (PET/CT): a feasibility study. Int J Radiat Oncol Biol Phys 2003;57:853–63.
69. Ling CC, Humm J, Larson S, Amols H, Fuks Z, Leibel S, et al. Towards multidimensional radiotherapy (MD-CRT): biological imaging and biological conformality. Int J Radiat Oncol Biol Phys 2000;47:551–60.
70. Schwartz DL, Ford EC, Rajendran J, Yueh B, Coltrera MD, Virgin J, et al. FDG-PET/CT-guided intensity modulated head and neck radiotherapy: a pilot investigation. Head Neck 2005;27:478–87.
71. Gilman MD, Fischman AJ, Krishnasetty V, Halpern EF, Aquino SL. Hybrid PET/CT of the thorax: when is computer registration necessary? J Comput Assist Tomogr 2007;31:395–401.
72. Greco C, Rosenzweig K, Cascini GL, Tamburrini O. Current status of PET/CT for tumour volume definition in radiotherapy treatment planning for non-small cell lung cancer (NSCLC). Lung Cancer 2007;57:125–34.
73. Messa C, Ceresoli GL, Rizzo G, Artioli D, Cattaneo M, Castellone P, et al. Feasibility of [18F]FDG-PET and coregistered CT on clinical target volume definition of advanced non-small cell lung cancer. Q J Nucl Med Mol Imaging 2005;49:259–66.
74. Deniaud-Alexandre E, Touboul E, Lerouge D, Grahek D, Foulquier JN, Petegnief Y, et al. Impact of computed tomography and 18F-deoxyglucose coincidence detection emission tomography image fusion for optimization of conformal radiotherapy in non-small-cell lung cancer. Int J Radiat Oncol Biol Phys 2005;63:1432–41.
75. Cherry SR. The 2006 Henry N. Wagner Lecture: Of mice and men (and positrons)—advances in PET imaging technology. J Nucl Med 2006;47:1735–45.
76. Townsend DW. Multimodality imaging of structure and function. Phys Med Biol 2008;53:R1–39.
77. Wong W, Zhang Y, Liu S, Li H, Baghaei H, Ramirez RA, et al. Feasibility studies of an affordable high resolution 1 meter long PET. J Nucl Med 2008;49(Suppl 1):4110.
78. Conti M, Bendriemj B, Casey M. Performance of a high sensitivity PET scanner based on LSO panel detectors. IEEE Trans Nucl Sci 2006;53:1136–42.
79. Watanabe M, Shimuzu K, Omura T. A high-throughput whole-body PET scanner using flat panel PS-PMTs. IEEE Trans Nucl Sci 2004;51:796–800.
80. Derenzo SE. Mathematical removal of positron range blurring in high-resolution tomography. IEEE Trans Nucl Sci 1986;33:565–9.
81. Moses WW, Derenzo SE, Melcher CL, Manente RA. A room temperature LSO/Pin photodiode PET detector module that measures depth of interaction. IEEE Trans Nucl Sci 1995;42:1085–9.
82. Dahlbom M, MacDonald LR, Eriksson L, Paulus M, Andreaco M, Casey ME, et al. Performance of a YSO/LSO phoswitch detector for use in a PET/SPECT system. IEEE Trans Nucl Sci 1998;44:1114–9.
83. Wienhard K, Schmand M, Casey ME, Baker K, Bao J, Eriksson L, et al. The ECAT HRRT: performance and first clinical application of the new high resolution research tomograph. IEEE Trans Nucl Sci 2002;49:104–10.
84. Stocklin GL. Is there a future for clinical fluorine-18 radiopharmaceuticals (excluding FDG)? Eur J Nucl Med 1998;25:1612–6.
85. Varagnolo L, Stokkel MP, Mazzi U, Pauwels EK. 18F-labeled radiopharmaceuticals for PET in oncology, excluding FDG. Nucl Med Biol 2000;27:103–12.
86. Shiue CY, Welch MJ. Update on PET radiopharmaceuticals: life beyond fluorodeoxyglucose. Radiol Clin North Am 2004;42:1033–1053. viii.
87. Couturier O, Luxen A, Chatal JF, Vuillez JP, Rigo P, Hustinx R. Fluorinated tracers for imaging cancer with positron emission tomography. Eur J Nucl Med Mol Imaging 2004;31:1182–206.
88. Vallabhajosula S. 18F-labeled positron emission tomographic radiopharmaceuticals in oncology: an overview of radiochemistry and mechanisms of tumor localization. Semin Nucl Med 2007;37:400–19.
89. Groves AM, Win T, Haim SB, Ell PJ. Non-[18F]FDG PET in clinical oncology. Lancet Oncol 2007;8:822–30.

90. Christensen N, Hammer B, Heil B, Fetterly K. Positron emission tomography within a magnetic field using phototubes and lightguides. Phys Med Biol 1995;40:691–7.
91. Buchanan M. A system to obtain radiotracer uptake data simultaneously with NMR spectra in a high field magnet. IEEE Trans Nucl Sci 1996;43:2044–8.
92. Shao Y, Cherry SR, Farahani K, Slates R, Silverman RW, Meadors K, et al. Development of a PET detector system compatible with MRI/NMR systems. IEEE Trans Nucl Sci 1997;44:1167–71.
93. Slates R, Cherry S, Boutefnouchet A, Shao Y, Dahlborn M, Farahani K. Design of a small animal MR compatible PET scanner. IEEE Trans Nucl Sci 1999;46:565–70.
94. Catana C, Wu Y, Judenhofer MS, Qi J, Pichler BJ, Cherry SR. Simultaneous acquisition of multislice PET and MR images: initial results with a MR-compatible PET scanner. J Nucl Med 2006;47:1968–76.
95. Judenhofer MS, Catana C, Swann BK, Siegel SB, Jung WI, Nutt RE, et al. PET/MR images acquired with a compact MR-compatible PET detector in a 7-T magnet. Radiology 2007;244:807–14.
96. Pichler BJ, Swann BK, Rochelle J, Nutt RE, Cherry SR, Siegel SB. Lutetium oxyorthosilicate block detector readout by avalanche photodiode arrays for high resolution animal PET. Phys Med Biol 2004;49:4305–19.
97. Pichler BJ, Judenhofer MS, Catana C, Walton JH, Kneilling M, Nutt RE. Performance test of an LSO-APD detector in a 7-T MRI scanner for simultaneous PET/MRI. J Nucl Med 2006;47:639–47.
98. Burbar Z, Graxioso R, Corbeil JL, et al. PET performance of PET/MR brain insert tomograph (abstract). Nuclear Science Symposium and Medical Imaging Conference Record, 2006. IEEE, p 116.
99. Schmand M, Burbar Z, Corbeil J, Zhang N, Michael C, Byars L, et al. BrainPET: first human tomograph for simultaneous (functional) PET and MR imaging. J Nucl Med 2007;48(Suppl 2):45P.
100. Schlemmer HP, Pichler BJ, Schmand M, Burbar Z, Michel C, Ladebeck R, et al. Simultaneous PET/MR imaging of the human brain: feasibility study. Radiology 2008;248:1028–35.
101. Kops RR, Qin P, Mueller-Veggian M, Herzog H. Attenuation correction of PET scanning based on MR images. Nuclear Science Symposium and Medical Imaging Conference Record, 2006, IEEE.
102. Hofmann M, Steinke F, Scheel V, Charpiat G, Brady M, Schoelkopf B, et al. MR-based PET attenuation correction – method and validation (abstract). Nuclear Science Symposium and Medical Imaging Conference, 2007, IEEE, M16-6.
103. Zaidi H, Mawlawi O, Orton CG. Point/counterpoint. Simultaneous PET/MR will replace PET/CT as the molecular multimodality imaging platform of choice. Med Phys 2007;34:1525–8.